Diagnosis of Track Forecast Errors for Tropical Cyclone Rita (2005) Using GEFS Reforecasts

THOMAS J. GALARNEAU JR.*

National Center for Atmospheric Research,+ Boulder, Colorado

THOMAS M. HAMILL

NOAA/Earth System Research Laboratory/Physical Sciences Division, Boulder, Colorado

(Manuscript received 20 March 2015, in final form 2 June 2015)

ABSTRACT

Analysis and diagnosis of the track forecasts for Tropical Cyclone (TC) Rita (2005) from the Global Ensemble Forecast System (GEFS) reforecast dataset is presented. The operational numerical weather prediction guidance and GEFS reforecasts initialized at 0000 UTC 20–22 September 2005, 2–4 days prior to landfall, were all characterized by a persistent left-of-track error. The numerical guidance indicated a significant threat of landfall for the Houston, Texas, region on 24 September. The largest mass evacuation in U.S. history was ordered, with the evacuation resulting in more fatalities than TC Rita itself. TC Rita made landfall along the Texas–Louisiana coastal zone on 24 September. This study utilizes forecasts from the GEFS reforecast and a high-resolution regional reforecast. The regional reforecast was generated using the Advanced Hurricane Weather Research and Forecasting Model (AHW) with the GEFS reforecasts providing the initial and boundary conditions. The results show that TC Rita's track was sensitive to errors in both the synoptic-scale flow and TC intensity. Within the GEFS reforecast ensemble, the nonrecurving members were characterized by a midlevel subtropical anticyclone that extended too far south and west over the southern United States, and an upper-level cutoff low west and anticyclone east of TC Rita that were too weak. The AHW regional reforecast ensemble further highlighted the role of intensity and steering-layer depth in TC Rita's track. While the AHW forecast was initialized with a TC that was too weak, the ensemble members that were able to intensify TC Rita more rapidly produced a better track forecast because the TCs followed a deeper steering-layer flow.

1. Introduction

The importance of accurate prediction of tropical cyclone (TC) track was underscored with the landfall of TC Rita near the Louisiana–Texas border on 24 September 2005. Nearly one month after the devastating landfall of TC Katrina near New Orleans, Louisiana, TC Rita threatened the Gulf Coast from southern Texas to southwestern Louisiana. TC Rita reached category 5 intensity on the Saffir–Simpson scale (Simpson 1974) early on 22 September, 2 days prior to landfall (Table 1). Operational numerical weather prediction models initialized at 0000 UTC 20–22 September consistently indicated that landfall would occur between Corpus Christi and Port Arthur, Texas (Figs. 1a–c, Table 2). The largest mass evacuation in U.S. history was ordered for the Houston, Texas, area on 21–22 September, resulting in gridlock on highways (Zhang et al. 2007). The traffic jams, combined with extreme surface temperatures, resulted in nearly 100 fatalities due to the evacuation alone, while seven fatalities were directly associated with TC Rita's landfall (Horswell and Hegstrom 2005; Knabb et al. 2006). The operational model track forecasts for TC Rita had a significant left-of-track error, as the observed storm made landfall over the Louisiana–Texas border (Figs. 1a–c). Given the consistent left-of-track forecast error and the socioeconomic impacts that accompanied TC Rita, this event is worthy of detailed analysis to

* Current affiliation: Department of Atmospheric Sciences, University of Arizona, Tucson, Arizona.

+ The National Center for Atmospheric Research is sponsored by the National Science Foundation.

Corresponding author address: Thomas J. Galarneau Jr., Department of Atmospheric Sciences, University of Arizona, P.O. Box 210081, Tucson, AZ 85721.
E-mail: tom.galarneau.jr@gmail.com

DOI: 10.1175/WAF-D-15-0036.1

TABLE 1. Hurricane Best-Track Database (HURDAT; Landsea et al. 2004) entries for TC Rita (2005) from Knabb et al. (2006). Abbreviations for the state of the system are remnant low (LO), tropical depression (TD), tropical storm (TS), and hurricane (HU). The latitude and longitude position, MSLP (hPa), and maximum wind speed (kt) are indicated. Initialization times and dates for the GEFS reforecasts and ARW regional reforecasts are set in boldface. The synoptic time and date closest to landfall is set in italics.

Hour (UTC)	Date	Lat (°N)	Lon (°W)	MSLP (hPa)	Wind speed (kt)	State
0000	18 Sep	21.3	69.9	1009	25	TD
0600	18 Sep	21.6	70.7	1009	25	TD
1200	18 Sep	21.9	71.5	1007	30	TD
1800	18 Sep	22.2	72.3	1005	35	TS
0000	19 Sep	22.4	73.0	1002	45	TS
0600	19 Sep	22.6	73.8	999	50	TS
1200	19 Sep	22.8	74.7	997	55	TS
1800	19 Sep	23.1	75.9	994	60	TS
0000	**20 Sep**	23.3	77.2	992	60	TS
0600	20 Sep	23.5	78.8	990	60	TS
1200	20 Sep	23.7	80.3	985	70	HU
1800	20 Sep	23.9	81.6	975	85	HU
0000	**21 Sep**	24.1	82.7	967	95	HU
0600	21 Sep	24.2	84.0	955	110	HU
1200	21 Sep	24.2	85.2	941	120	HU
1800	21 Sep	24.3	86.2	920	145	HU
0000	**22 Sep**	24.5	86.9	897	150	HU
0600	22 Sep	24.8	87.6	897	155	HU
1200	22 Sep	25.2	88.3	908	140	HU
1800	22 Sep	25.6	89.1	914	125	HU
0000	23 Sep	26.0	89.9	915	120	HU
0600	23 Sep	26.5	90.7	924	115	HU
1200	23 Sep	27.1	91.5	927	115	HU
1800	23 Sep	27.8	92.3	930	110	HU
0000	24 Sep	28.6	93.0	931	105	HU
0600	*24 Sep*	29.4	93.6	935	100	HU
1200	24 Sep	30.5	94.1	949	65	HU
1800	24 Sep	31.6	94.1	974	45	TS
0000	25 Sep	32.7	94.0	982	35	TS
0600	25 Sep	33.7	93.6	989	30	TD
1200	25 Sep	34.7	92.5	995	25	TD
1800	25 Sep	35.8	91.4	1000	25	TD
0000	26 Sep	37.0	90.1	1003	20	TD
0600	26 Sep	39.5	88.0	1006	20	LO

determine factors that contributed to the left-of-track forecast errors within the context of climatological track forecast errors in the Gulf of Mexico region.

The impacts of forecast errors on the structure and evolution of synoptic-scale weather systems on TC track forecasts are well documented (e.g., Carr and Elsberry 2000; Majumdar et al. 2006; Wu et al. 2009). Over the tropical North Atlantic in particular, the motion of TCs is influenced by the position and structure of the subtropical anticyclone (Mitchell 1924). Torn and Davis (2012) showed that prediction of the subtropical anticyclone in the Advanced Hurricane Weather Research and Forecasting Model (AHW; Skamarock et al. 2008; Davis et al. 2010) was sensitive to the treatment of shallow convection by cumulus parameterizations. In a case similar to that of TC Rita, Brennan and Majumdar (2011) showed that the forecast track of TC Ike (2008) was sensitive to the structure and westward extent of the subtropical anticyclone over the southeastern United States. In their study, the operational numerical guidance initialized at 0000 UTC 9 September 2008 all steered Ike into southern Texas, rather than recurved Ike farther north toward Houston. This left-of-track forecast error was attributed to increased zonal elongation of the subtropical ridge over the southeastern United States and its attendant easterly steering flow over the Gulf of Mexico. Komaromi et al. (2011) suggested that these errors in synoptic-scale flow originated as errors in the initial conditions. Clearly, errors in the synoptic-scale flow can be driven by initial condition and model physics errors.

The aim of this paper is to diagnose the numerical model forecast errors that contributed to the persistent left-of-track bias noted for TC Rita (2005; Figs. 1a–c).

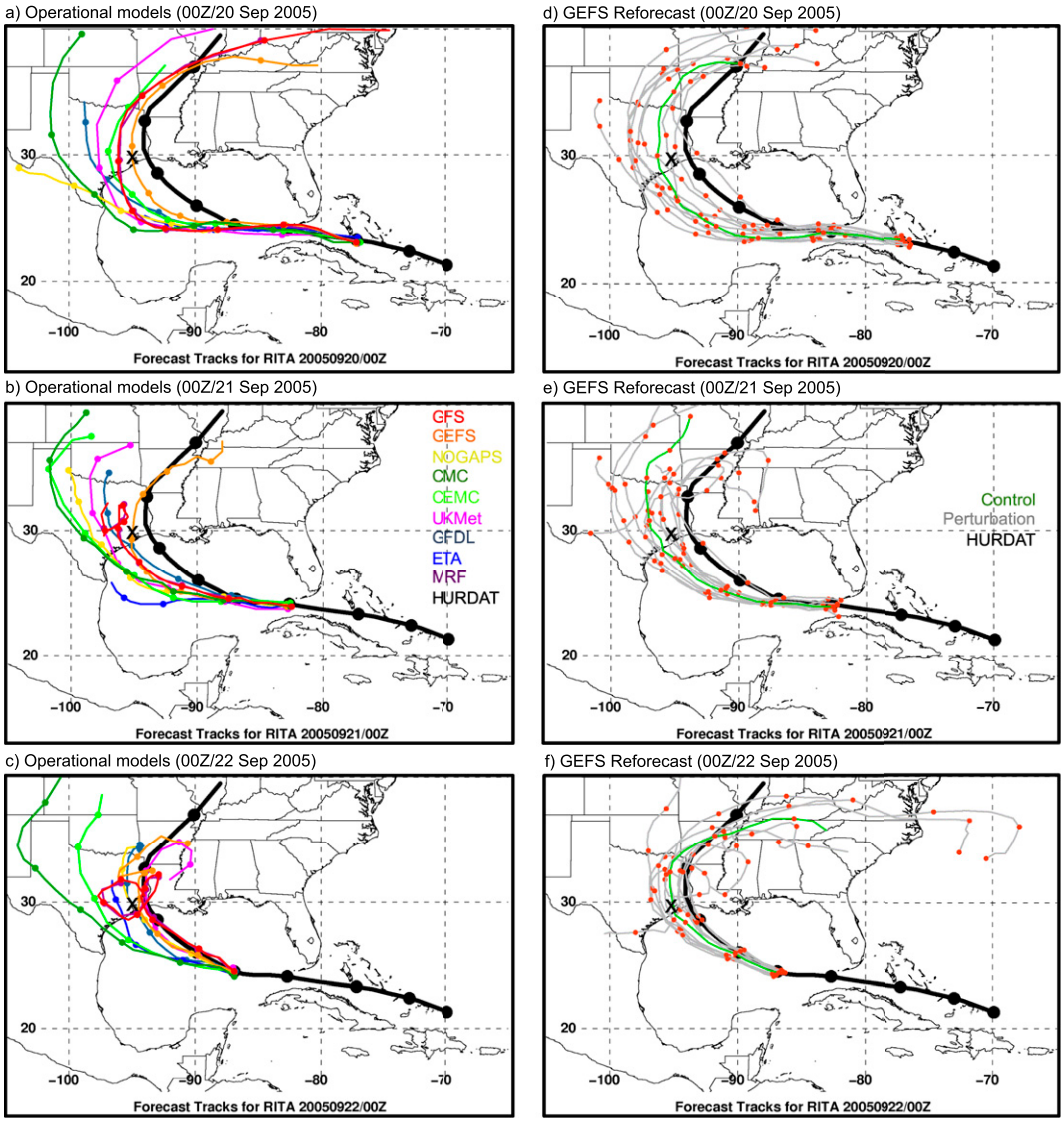

FIG. 1. TC Rita track forecasts from the 2005 operational numerical weather prediction models initialized at 0000 UTC (a) 20, (b) 21, and (c) 22 Sep 2005. The tracks are color coded according to the key in (b) (the model acronyms are summarized in Table 1), and the positions are labeled every 24 h at 0000 UTC by filled circles. (d)–(f) As in (a)–(c), but for the TC track forecasts from the GEFS reforecasts. The observed TC track is shown in black. The location of Houston is marked with a cross.

We will use the National Oceanic and Atmospheric Administration's (NOAA) global medium-range ensemble reforecast dataset, which consists of an 11-member ensemble forecast initialized at 0000 UTC daily from December 1984 to the present (Hamill et al. 2013). The value of using reforecasts is that the long time period covered using a current-generation global ensemble system allows for examination of forecast characteristics of relatively rare events, such as TCs, to determine if any persistent model errors occur. The reforecasts show a similar left-of-track behavior (Figs. 1d–f) as the 2005 operational models for the 0000 UTC 20–22 September initializations, indicating that despite expected improvements that accompany a more modern version of an ensemble numerical weather prediction system, forecasts for TC Rita were not markedly changed or improved.

To provide context for the track forecasts for TC Rita, the reforecast ensemble-mean climatological track and intensity forecast error for TCs over the Gulf of Mexico during 1985–2010 is shown in Fig. 2. To be included in the verification statistics, the TC of interest is located over the Gulf of Mexico north of 20°N and west of 81°W at the verifying time. The mean absolute error (km;

TABLE 2. Summary of operational numerical model track forecasts for TC Rita (2005) shown in Figs. 1a–c. The NCEP Eta and MRF modeling systems have since been retired.

Model acronym	Description
GFS	NCEP Global Forecast System global model
GEFS	NCEP Global Ensemble Forecast System
NOGAPS	U.S. Navy Operational Global Atmospheric Prediction System global model
CMC	Canadian Meteorological Centre global model (GEM)
CEMC	CMC ensemble mean
UKMet	Met Office global model
GFDL	Geophysical Fluid Dynamics Laboratory hurricane model
ETA	NCEP Eta Model
MRF	NCEP Medium-Range Forecast Model

Fig. 2a) is not significantly different at any forecast lead time from the track error ''baseline'' established as part of the Hurricane Forecast Improvement Program (HFIP), calculated from the top-flight operational models for the 2006–08 North Atlantic TC seasons (Gall et al. 2014). Examination of the forecast track bias [computed in track-relative coordinates as shown by Buckingham et al. (2010), their Fig. 3] reveals a distinct slow and left-of-track error for forecast leads between 72 and 144 h (Fig. 2b). The bias prior to 72 h is small, with magnitudes near 25 km, while the bias after 144 h is slow and right of track. The track forecast bias for 26 yr of TC forecasts is consistent with the forecasts for TC Rita, all of which are characterized by a left-of-track error for all forecast leads and a slow error after 60 h (Fig. 2c). For intensity, the reforecasts are characterized by a negative bias significantly different from zero at all forecast leads (Fig. 2d), which is not surprising given the relatively coarse resolution of the global model. The influence of intensity on the track forecasts for TC Rita will be examined.

In addition to using global reforecast ensemble data, we will utilize a high-resolution explicit regional reforecast ensemble from AHW. The AHW ensemble, initialized at 0000 UTC 22 September 2005, is used to examine the impact of higher resolution on track forecasts for TC Rita. Additionally, AHW will help examine the impact of intensity and steering-layer depth on the track of TC Rita. The analysis of both the global reforecasts and a regional reforecast, and the linkages between these two modeling frameworks, will allow for a more complete interpretation of the factors that contributed to the left-of-track forecast errors for TC Rita in the 2–4-day period prior to landfall.

This paper is organized as follows. Section 2 provides a description of the forecast systems and diagnostic calculations used. Section 3 provides a brief synoptic analysis of TC Rita's life cycle, while section 4 describes the diagnosis of track forecasts from the global reforecast ensemble. Analysis of the AHW regional reforecast ensemble is presented in section 5. Section 6 provides the conclusions.

2. Data and methods

The NOAA global reforecast ensemble data were computed using the February 2012 operational version of the National Centers for Environmental Prediction (NCEP) Global Ensemble Forecast System (GEFS), version 9.0.1. The 11-member (10 perturbed members and a control forecast) reforecast ensemble was generated once daily at 0000 UTC from December 1984 to the present. Through 20 February 2011, the Climate Forecast System Reanalysis (CFSR; Saha et al. 2010) was used as initial conditions for the control member. After that, the initial conditions were generated from the NCEP operational analysis system. The reforecast ensemble was integrated at a resolution of T254L42 (approximately 40 km) through day 8, degrading to T190L42 (approximately 54 km) for days 8–16. Hamill et al. (2013) provide a complete description of the reforecast ensemble data and generation of the TC track forecasts.

Given the consistent left-of-track error among the reforecast ensemble for the forecasts initialized at 0000 UTC 20–22 September 2005 (Figs. 1d–f), a time-lagged ensemble approach is used (e.g., Schumacher and Galarneau 2012). Among the 33 ensemble members that comprise all forecasts for these initial times, the forecasts are classified based on the location of TC Rita at 0000 UTC 24 September. The 10 ensemble members at the farthest west longitudes are classified as ''left'' members, or nonrecurving. Likewise, the 10 ensemble members at the farthest east longitudes are classified as ''right'' members, or recurving. The remaining 13 members are classified as ''middle'' members. The number of ensemble members in each class at each initial time is summarized in Table 3. The nonrecurving and recurving ensemble members will be compared in section 4.

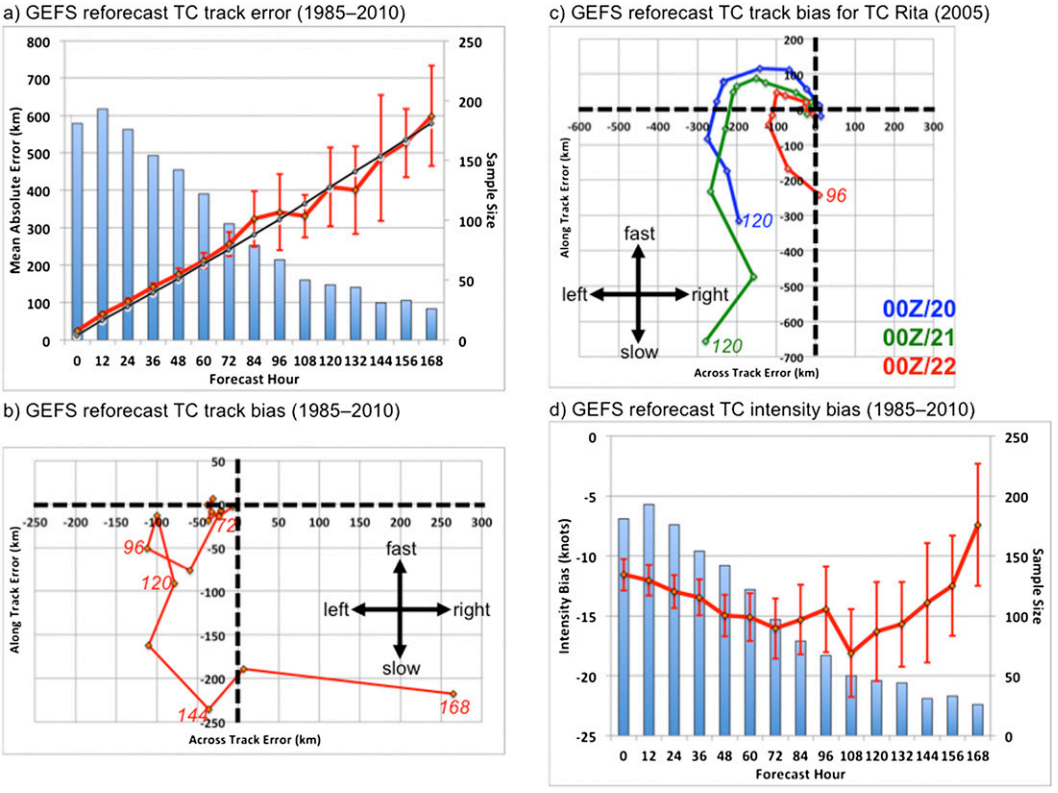

FIG. 2. TC track and intensity statistics in the Gulf of Mexico region from the GEFS reforecasts for 1985–2010. (a) The mean absolute error of the track (km; red line), HFIP "baseline" (km; black line), and sample size (blue bars); (b) track forecast bias (km; red line) in TC track–relative coordinates; (c) track forecast bias for TC Rita initialized at 0000 UTC 20 (blue), 21 (green), and 22 (red) Sep 2005; and (d) intensity bias (kt; red line) and sample size (blue bars). The error bars in (a) and (d) represent the 90% confidence interval.

The 11-member AHW regional reforecast ensemble 72-h forecast, initialized at 0000 UTC 22 September 2005, was generated using version 3.6.1 of the Advanced Research version of the Weather Research and Forecasting Model with modifications for TC applications (Davis et al. 2010). The configuration of AHW used here is summarized in Table 4. The numerical forecasts were made using 51 vertical levels up to 20 hPa over an outer domain of 36-km (320 × 210 grid points) horizontal grid spacing (Fig. 3). Moving two-way inner nests of 12 km (133 × 133 grid points) and 4 km (199 × 199 grid points) centered on TC Rita were used. The movement of the inner nests every 15 min during the model integration was determined by TC Rita's movement during the previous 15 min. The initial and lateral boundary conditions (updated every 3 h) were derived from the corresponding GEFS reforecast ensemble member.

We used vorticity inversion to compute the environment wind and steering-layer flow for TC Rita, with Rita's cyclonic circulation removed. A Poisson solver was used to invert the vorticity and divergence as

$$\nabla^2\psi = \begin{pmatrix} \zeta & \text{for} & r \le r_0 \\ 0 & \text{for} & r > r_0 \end{pmatrix} \tag{1}$$

and

$$\nabla^2\chi = \begin{pmatrix} \delta & \text{for} & r \le r_0 \\ 0 & \text{for} & r > r_0 \end{pmatrix}, \tag{2}$$

where ψ is the streamfunction, χ is the velocity potential, ζ is the relative vorticity, δ is the divergence, and r_0 is the radius at which the TC was removed. From the solutions of (1) and (2), the nondivergent and divergent wind vectors were computed as

TABLE 3. Count of time-lagged ensemble members based on the classification of forecast track for Rita for the 0000 UTC 20–22 Sep 2005 GEFS reforecasts.

Classification	20 Sep	21 Sep	22 Sep	Total
Left members (nonrecurving)	6	4	0	10
Middle members	3	5	5	13
Right members (recurving)	2	2	6	10
Total	11	11	11	33

TABLE 4. AHW, version 3.6.1, specifics. Multiple entries indicate model configurations for domains 1–3. The model domains are depicted in Fig. 3.

Model parameter	Configuration
Horizontal grid spacing (km)	36.0, 12.0, 4.0
Vertical levels	51, 51, 51
Time step (s)	180, 60, 20
Initialization time	0000 UTC 22 Sep 2005
Forecast length (h)	72
Initial and boundary condition	T254/L42 GEFS reforecast ensemble members (3-h updates)
Cumulus parameterization	Tiedtke, Tiedtke, none
Boundary layer	Yonsei University (YSU; Hong et al. 2006)
Microphysics	WRF single-moment 6-class microphysics scheme (WSM6; Hong et al. 2004)
Land surface	Noah (Ek et al. 2003)
Turbulence	2D Smagorinsky
Diffusion	Second-order diffusion
Scalar advection	Positive definite
Radiation (long- and shortwave)	Rapid Radiative Transfer Model for GCMs (RRTMG)

$$\mathbf{v}_{\psi} = \hat{k} \times \nabla\psi \tag{3}$$

and

$$\mathbf{v}_{\chi} = \nabla\chi. \tag{4}$$

The environment wind $\mathbf{v}_{\text{env}}$ with the effect of TC Rita removed for a given r_0 was then computed as

$$\mathbf{v}_{\text{env}} = \mathbf{v} - \mathbf{v}_{\psi} - \mathbf{v}_{\chi}, \tag{5}$$

where $\mathbf{v}$ was the total wind. The steering-layer flow was defined as the area- and vertically averaged $\mathbf{v}_{\text{env}}$ that best matched TC Rita's motion based on positions at ±12 h (Galarneau and Davis 2013). The vertical extent of the steering layer ranged from 50 to 650 hPa, with a fixed bottom at 850 hPa. Following the methodology of Galarneau and Davis (2013), analysis of the synoptic-scale $\mathbf{v}_{\text{env}}$ and steering-layer flow in the AHW forecasts are performed on the 36-km outer domain.

3. Synoptic analysis

The synoptic-scale flow pattern on 18–25 September 2005 (as represented by the 300–200-hPa layer–mean streamfunction) was characterized by an anticyclone over the south-central and southeastern continental United States (CONUS), with flanking troughs located over the western and eastern CONUS (Fig. 4). TC Rita

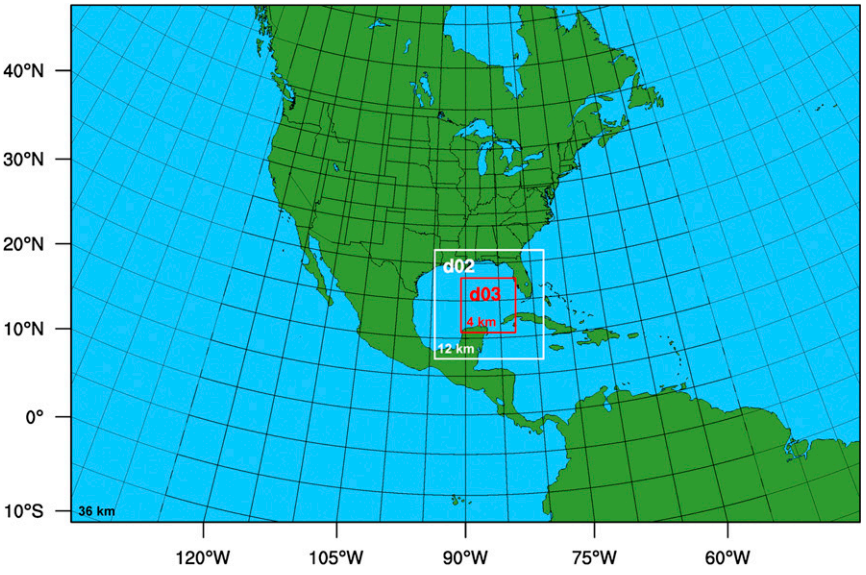

FIG. 3. Geographical locations of the AHW domains. The horizontal grid spacing on the parent domain is 36 km, and on the inner domains it is 12 and 4 km. The two inner domains are two-way moving nests centered on TC Rita.

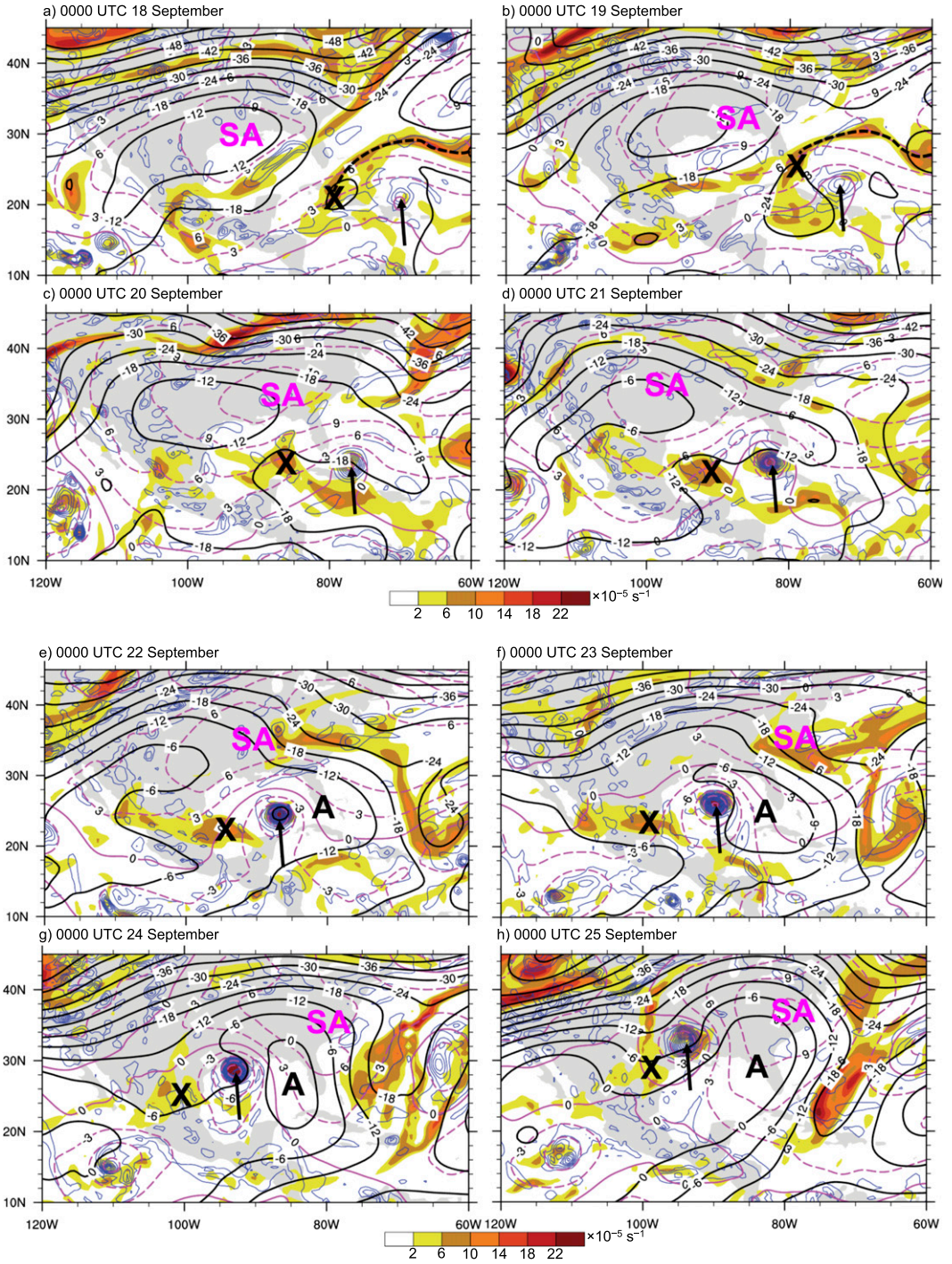

FIG. 4. CFSR 300–200-hPa layer–mean relative vorticity ($\times 10^{-5}\,s^{-1}$; shaded according to the color bar) with streamfunction ($\times 10^{6}\,m^{2}\,s^{-1}$; black contours with an interval of $6.0 \times 10^{6}\,m^{2}\,s^{-1}$), and 700–500-hPa layer–mean relative vorticity ($\times 10^{-5}\,s^{-1}$; blue contours with an interval of $4.0 \times 10^{-5}\,s^{-1}$ starting at $2.0 \times 10^{-5}\,s^{-1}$) with streamfunction ($\times 10^{6}\,m^{2}\,s^{-1}$; dashed magenta contours with an interval of $3.0 \times 10^{6}\,m^{2}\,s^{-1}$) at 0000 UTC (a) 18, (b) 19, (c) 20, (d) 21, (e) 22, (f) 23, (g) 24, and (h) 25 Sep 2005. TC Rita is labeled with a black arrow. The subtropical anticyclone over the southern CONUS is labeled with an SA, the upper-level anticyclone east of Rita is labeled with an A, and the cutoff low west of TC Rita is labeled with an X.

developed over the western North Atlantic on 18 September as an African easterly wave interacted with an upper-level potential vorticity (PV) streamer (Fig. 4a). TC Rita gradually intensified as it approached the Straits of Florida on 19–20 September (Figs. 4b,c, Table 1). Concurrently, the southwestern end of the upper-level PV streamer instrumental in TC Rita's initial development fractured into a cutoff low (labeled with an X) and moved westward into the Gulf of Mexico ahead of TC Rita. By 0000 UTC 21 September, TC Rita was in the midst of a rapid intensification period as it moved into the eastern Gulf of Mexico and the upper-level cutoff low was located over the southwestern Gulf of Mexico (Fig. 4d, Table 1).

At 0000 UTC 22 September, TC Rita was near its peak intensity at category 5 on the Saffir–Simpson scale while located over the east-central Gulf of Mexico (Fig. 4e, Table 1). At the synoptic scale, the subtropical ridge (labeled with an SA; as represented by 850–700-hPa layer–mean streamfunction) extended from the western North Atlantic to west-central Texas, and was associated with low- to midlevel easterly flow over the Gulf of Mexico. In the upper troposphere, the cutoff low was located over the extreme western Gulf of Mexico west of TC Rita, and a developing upper-level anticyclone (labeled with an A) was approximately centered over Florida east of TC Rita (Fig. 4e). The upper-level anticyclone developed southeast of a weak trough located over the eastern CONUS and was enhanced by diabatically driven upper-level anticyclogenesis associated with the rapid intensification of TC Rita.

On 22–25 September, TC Rita weakened to category 3 intensity as it moved northwestward and made landfall along the Texas–Louisiana coastal zone (Figs. 4e–h, Table 1). The key synoptic-scale circulation features that steered TC Rita northwestward are the cutoff low (labeled with an X) and anticyclone (labeled with an A) that flanked TC Rita at upper levels and the subtropical anticyclone (labeled with an SA) over the southeastern CONUS. The former two circulation features drove a southerly flow in the upper levels and the latter drove an easterly flow in the low to midlevels. The resulting southwesterly deep-layer vertical wind shear likely contributed to TC Rita's weakening and a more northwestward course on 23–24 September.

In the following sections, we will examine factors that contributed to the persistent left-of-track error in the GEFS reforecasts and the AHW regional reforecast. Specifically, we will address why the numerical model forecasts failed to readily recurve TC Rita on 22–24 September. We will assess the relative roles of forecast errors in synoptic-scale circulation features, and TC intensity and steering-layer depth in driving TC Rita on a more westward course (toward Houston) than observed.

4. GEFS reforecasts

In this section, we will examine the GEFS track reforecasts for TC Rita initialized at 0000 UTC 20–22 September 2005. As discussed earlier, the track forecasts are characterized by a left-of-track error for all three forecast initialization times, which is similar to the climatological forecast track bias over the Gulf of Mexico for 1985–2010 (Figs. 1d–f and 2b). Note that 27 of 33 ensemble members that composed the three initialization times to be analyzed are characterized by a left-of-track error, defined by the longitude of TC Rita at 0000 UTC 24 September (Fig. 5a). This result is consistent with the global TC track error and spread statistics presented by Hamill et al. (2013; see their Fig. 2), which showed that the GEFS reforecasts are underdispersive. The distribution of the forecast longitude of TC Rita at 0000 UTC 24 September shows that nearly all of the ensemble members had a left-of-track position at 96- and 72-h forecast leads (Fig. 5b). For 48-h forecast leads from the 0000 UTC 22 September initialization, there is a significant[1] eastward shift in the distribution of longitude, indicating an abrupt improvement over previous forecasts. This improvement is related to improved representation of the upper-level anticyclone northeast of TC Rita at 0000 UTC 22 September 2005 (not shown). Note, however, that the track forecast errors are still predominantly left of track.

Although the ensemble-mean global TC track forecasts for 1985–2010 are underdispersive in the GEFS reforecasts (Hamill et al. 2013), using a time-lagged ensemble approach adds to the range of possible outcomes. Note that when considering all ensemble members from the 0000 UTC 20–22 September initializations, the envelope of landfall points for TC Rita ranges from southeastern Texas between Brownsville and Corpus Christi to southern Louisiana just west of Vermilion Bay (Figs. 1d–f). To determine factors that influenced TC Rita's forecast track among the ensemble members, we will use ensemble synoptic analysis following methods similar to those of Hakim and Torn

[1] Unless otherwise noted, statistical significance was assessed using the Wilcoxon–Mann–Whitney rank sum test (Wilks 1995, 138–143) with significance defined at the 95% level. A nonparametric test was used to account for skewness in the data distributions.

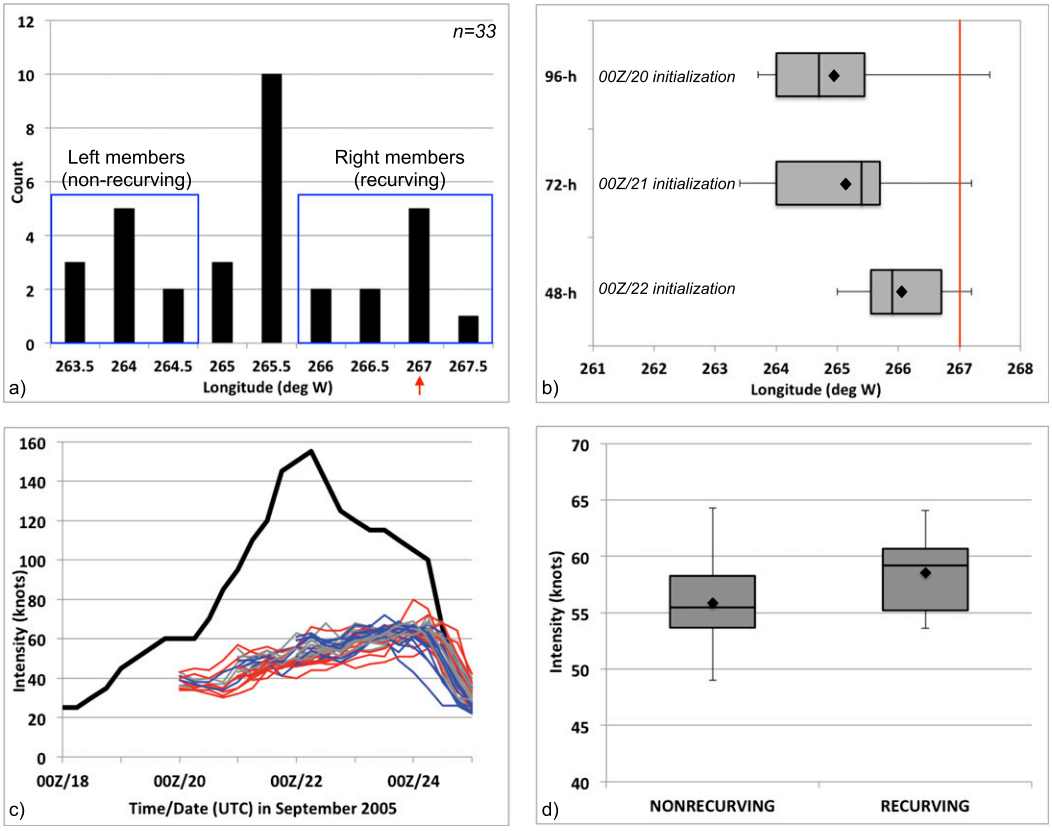

FIG. 5. TC track and intensity statistics from the GEFS reforecasts initialized at 0000 UTC 20–22 Sep 2005. (a) Histogram of TC Rita's longitude at 0000 UTC 24 Sep. The nonrecurving and recurving members are labeled with a blue box and the observed TC longitude is labeled with a red arrow. (b) Box-and-whiskers plot of forecasted TC longitude at 0000 UTC 24 Sep. The lower and upper bounds of the box mark the 25th and 75th percentiles, respectively. The black line within the box marks the median and the black diamond marks the mean. The whiskers indicate the max and min values, and the red line marks the observed TC longitude. (c) Time series of intensity (kt) for the observed TC (black line) with the nonrecurving (red line), recurving (blue line), and middle (gray line) ensemble members. (d) As in (b), but for TC intensity (kt) in the nonrecurving and recurving ensembles.

(2008), Schumacher and Galarneau (2012), and Torn et al. (2015). Specifically, we will compare the 10 nonrecurving and 10 recurving ensemble members through composite mean fields. Note that all of the ensemble members have a negative intensity bias reaching nearly 100 knots (kt; $1\,\text{kt} = 0.51\,\text{m}\,\text{s}^{-1}$) by 0600 UTC 22 September (Fig. 5c). The negative intensity bias is significantly worse than climatology over the Gulf of Mexico (Fig. 2d). Comparing the nonrecurving and recurving ensemble members, there is a suggestion that the recurving ensemble members produce a slightly stronger TC, but the intensity differences among the two ensemble groups are not significant (Fig. 5d).

The time-mean 250-hPa geopotential height for 0000 UTC 22–23 September 2005 shows that TC Rita moved northwestward in an environment with an anticyclone over the southern plains and east of TC Rita over Florida and the northern Caribbean (Fig. 6a). The relatively lower heights over Mexico were collocated with the upper-level cutoff low (see also Figs. 4e,f). The recurving ensemble member composite has relatively small 250-hPa height errors in the vicinity of TC Rita, with height errors generally less than 6 m except for directly over the TC (Fig. 6b). The nonrecurving composite is characterized by larger 250-hPa height errors in both midlatitudes and near the TC (Fig. 6c). The height error pattern in the midlatitudes, with positive errors in the trough over the western CONUS and negative errors in the ridge axis over the Great Lakes and southern Canada, is consistent with a more zonal waveguide with reduced meridional flow making it more difficult to steer a TC poleward. Near the TC, the nonrecurving composite shows a positive height error west of TC Rita, indicating that the cutoff low (labeled with an X in

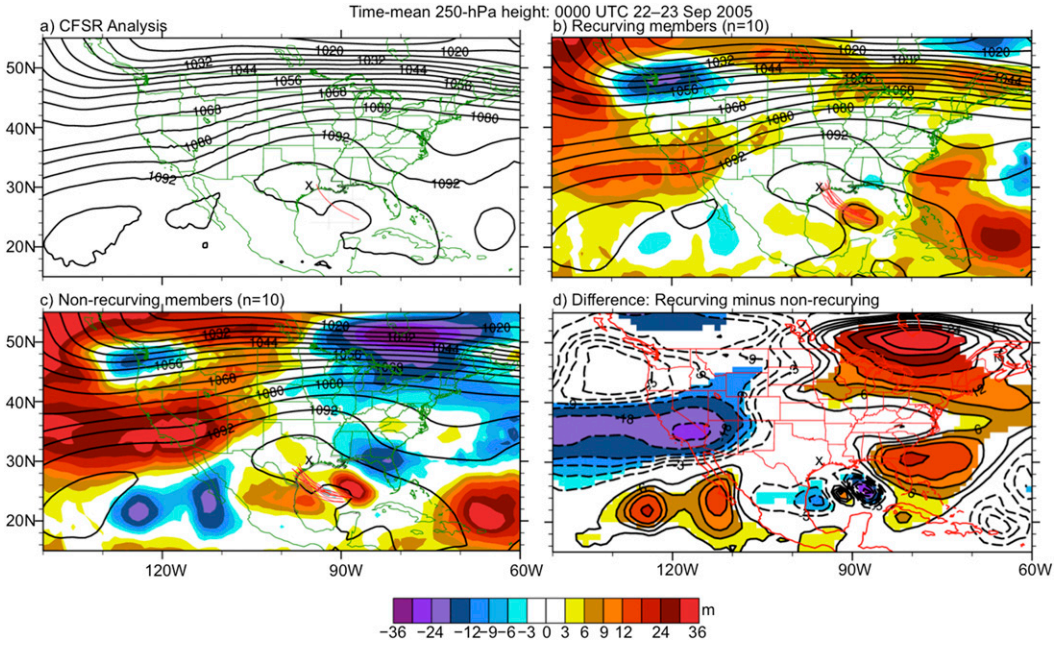

FIG. 6. The time-mean 250-hPa geopotential height (dam; black contours with an interval of 6 dam) at 0000 UTC 22–23 Sep 2005 from (a) CFSR and the (b) recurving and (c) nonrecurving ensembles. The ensemble-mean 250-hPa geopotential height error (forecast minus CFSR analysis; m; shaded according to the color bar) is shown in (b) and (c). The observed track (red line) of TC Rita from 0000 UTC 22 Sep to 1200 UTC 24 Sep 2005 is shown in (a), and the forecast tracks (red lines) for the same period for the nonrecurving and recurving ensemble are shown in (b) and (c). (d) The 250-hPa geopotential height difference (recurving minus nonrecurving) between the two ensemble groups (m; shading according to the color bar with solid contours indicating positive and dashed contours indicating negative). The height differences are shaded where statistically significant at the 95% confidence level using bootstrap resampling without replacement. The location of Houston is labeled with an X.

Fig. 4) is too weak in the forecast. Negative height errors are located over Florida and the eastern Gulf of Mexico, indicating that the upper-level anticyclone is weaker in the forecast. Both of these errors are consistent with reduced meridional flow over the Gulf of Mexico. The positive height error over the central Gulf of Mexico immediately northeast of the TC is a signature of the TC position error in the forecast.

Comparing the recurving and nonrecurving composites, the recurving ensemble members have a stronger cutoff low over the western Gulf of Mexico and a stronger anticyclone over Florida and the extreme eastern Gulf of Mexico (Fig. 6d). These height differences are significant at the 95% level using bootstrap resampling without replacement.[2] The positive–negative height difference couplet over the central Gulf of Mexico is a signature of the TC position difference between the two ensemble groups.

To relate the nonrecurving and recurving ensemble geopotential height differences to the environment wind (i.e., $\mathbf{v}_{env}$), the ensemble-mean streamlines and wind speed verifying at 1200 UTC 22 September 2005 are shown in Fig. 7. The verifying time shown coincides with the initial departure in TC motion between the two ensemble groups. To compute $\mathbf{v}_{env}$, vorticity inversion is used to remove the TC[3] in each ensemble member prior to compositing. Distinct differences are apparent in the $\mathbf{v}_{env}$ streamlines among the two ensemble groups. At 200 hPa, the anticyclone centered over southern Florida and the cutoff low over eastern Mexico are better defined and both have stronger circulation in the recurving ensemble compared to the nonrecurving ensemble (Figs. 7a,b). As a result, the 200-hPa $\mathbf{v}_{env}$ has more of a southerly component over TC Rita compared to the nonrecurving composite. The anticyclone over southern

[2] Two subsets of 10 ensemble members were randomly selected from the 33-member time-lagged ensemble and the 250-hPa height difference between the ensemble means of the two subsets was calculated. This calculation was repeated 10 000 times to obtain the 95% confidence bounds on the composite difference.

[3] Vorticity inversion is employed using a TC removal radius of 4°.

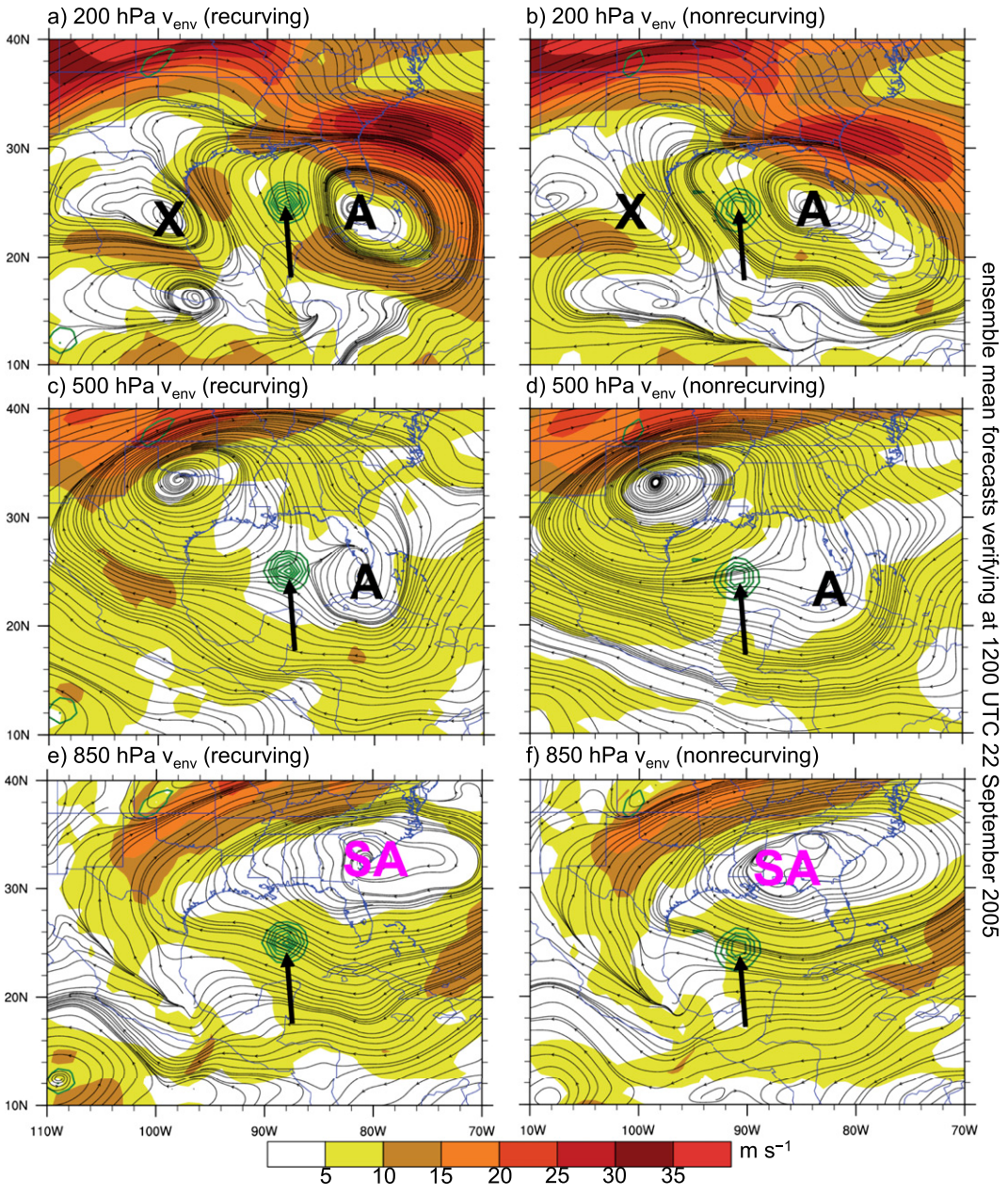

FIG. 7. Ensemble-mean $\mathbf{v}_{env}$ speed (m s^{-1}; shaded according to the color bar) and streamlines (black curved lines) for the (left) recurving and (right) nonrecurving ensembles at (a),(b) 200; (c),(d) 500; and (e),(f) 850 hPa verifying at 1200 UTC 22 Sep 2005. The TC was removed using vorticity inversion out to a radius of 4°. To show where TC Rita was located within the environment flow, the ensemble-mean 925–850-hPa layer–mean relative vorticity ($\times 10^{-5}$ s^{-1}; green contours with an interval of 4.0×10^{-5} s^{-1} starting at 4.0×10^{-5} s^{-1}) is plotted. Key circulation features are marked as in Fig. 4.

Florida is also a deeper circulation that is well defined at 500 hPa in the recurving composite (Fig. 7c). The circulation is a weaker open-wave structure at 500 hPa in the nonrecurving composite (Fig. 7d). At 500 hPa, TC Rita is embedded in a weak deformation flow between the anticyclones over southern Florida and northern Texas in the recurving composite. In the nonrecurving composite, TC Rita is embedded in easterly flow. The scatterplot of the $\mathbf{v}_{env}$ components at 500 hPa for all of the ensemble members shows that the nonrecurving ensemble members have significantly stronger easterly flow at 500 hPa (Fig. 8a). The ~1.0 m s^{-1} difference in 500-hPa $\mathbf{v}_{env}$ translates to a TC position error of nearly 100 km day^{-1}.

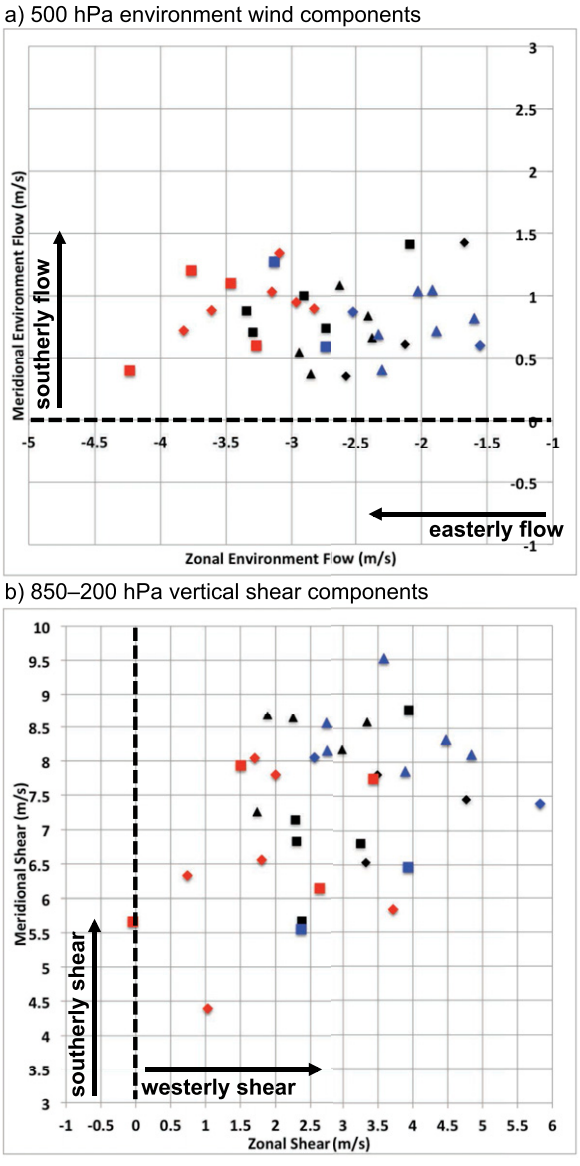

FIG. 8. Scatterplot of zonal u and meridional v components of the time-mean (a) 500-hPa $\mathbf{v}_{env}$ ($m\,s^{-1}$) and (b) 850–200-hPa vertical wind shear ($m\,s^{-1}$) at 0000 UTC 22–23 Sep 2005. The nonrecurving members are highlighted in red and recurving members are in blue. The ensemble members were initialized at 0000 UTC 20, 21, and 22 Sep and are marked by filled diamonds, squares, and triangles, respectively.

Comparison of the 850-hPa $\mathbf{v}_{env}$ between recurving and nonrecurving ensembles shows that in both groups, TC Rita is embedded in easterly flow on the southern flank of the subtropical anticyclone over the southern CONUS (Figs. 7e,f). The center of the subtropical anticyclone circulation is located farther west in the nonrecurving ensemble compared to the recurving ensemble. This result is similar to that for TC Ike, as documented by Brennan and Majumdar (2011), where TC track is sensitive to the position and westward extent of the subtropical anticyclone. The easterly $\mathbf{v}_{env}$ at 850 hPa combined with differences in $\mathbf{v}_{env}$ at 200 hPa results in significant differences in the deep-layer vertical wind shear between the recurving and nonrecurving ensemble groups (Fig. 8b). The recurving ensemble is characterized by stronger southwesterly vertical shear compared to the nonrecurving ensemble. The larger deep-layer vertical shear and weaker 500-hPa easterly flow both favor a more northwestward track.

In summary, the forecast tracks of TC Rita by the GEFS reforecasts were characterized by a persistent left-of-track error that was both consistent with track forecasts from the operational models in 2005 and the GEFS reforecast climatological track forecast bias over the Gulf of Mexico for 1985–2010. While differences in the forecast intensity of TC Rita differed slightly among the GEFS reforecast ensemble members initialized at 0000 UTC 20–22 September, significant differences in the structure of nearby synoptic-scale weather systems modulated the track of TC Rita. In comparing the subset of recurving and nonrecurving ensemble members using a time-lagged ensemble approach similar to Schumacher and Galarneau (2012), we determined that TC Rita's track was influenced by the (i) position and westward extent of the subtropical anticyclone over the southern CONUS, (ii) intensity and position of the upper-level cutoff low over eastern Mexico, and (iii) intensity and depth of the upper-level anticyclone east of TC Rita. While the latter synoptic-scale circulation feature was influenced by diabatically driven upper-level anticyclogenesis as TC Rita rapidly intensified, it is not clear if differences in the anticyclone structure and intensity within the ensemble were modulated by this effect. The intensity of TC Rita was not significantly different among the ensemble groups.

In the next section, we will use an AHW regional reforecast to examine the impact of increased resolution and differences in steering-layer depth and intensity on the track forecasts for TC Rita.

5. AHW regional reforecast

In this section, we will examine the track forecasts from a high-resolution AHW regional reforecast ensemble initialized at 0000 UTC 22 September 2005, about 60 h prior to TC Rita's landfall. The AHW ensemble forecasts use the GEFS reforecast initialized at 0000 UTC 22 September as initial and lateral boundary conditions. The AHW track and intensity forecasts are shown in Fig. 9. Note that despite the increased resolution of AHW, the track forecasts show little difference

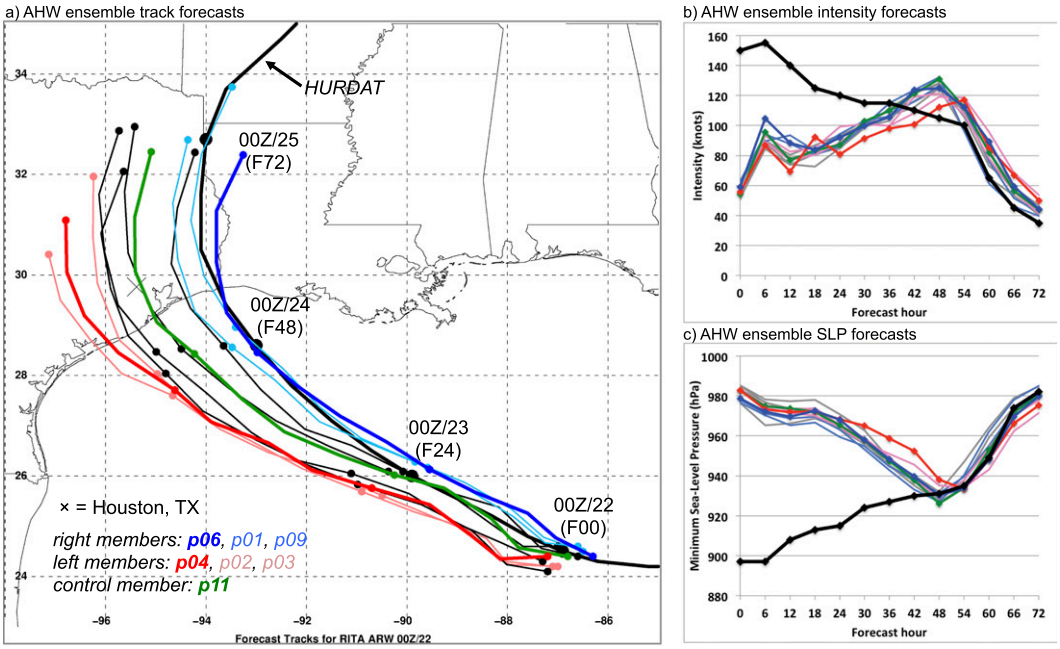

FIG. 9. (a) Track, (b) intensity (kt), and (c) MSLP (hPa) forecasts from the 72-h AHW regional reforecast ensemble initialized at 0000 UTC 22 Sep 2005. The observed TC is marked by the thick black line. In (a), the three leftmost members are in red, the rightmost perturbation members are in blue, and the control member is in thick green. The representative left- (p_{04}) and rightmost (p_{06}) ensemble members are marked by a thick line. All other ensemble members are in thin black. The track positions are labeled every 24 h at 0000 UTC. The location of Houston is labeled with an X.

compared to the GEFS reforecasts (cf. with Fig. 1f). In the control forecast, TC Rita made landfall near Houston at ~0600 UTC 24 September (Fig. 9a). For the perturbed ensemble members, the landfall points range from Port Lavaca, Texas, to Port Arthur, covering 300 km of coastline left of the observed track. Comparison of the TC motion error for the control member (green track), left perturbation member p_{04} (thick red track), and right perturbation member p_{06} (thick blue track) of the 12–60-h forecast is shown in Fig. 10. The control and left perturbation members are characterized by a southwestward motion error near 1.5 m s^{-1} after 18 h, while the right perturbation member has lower motion errors overall. The southwestward motion error is indicative of a more westward track, delayed recurvature, and landfall farther south along the Texas coastline (Figs. 9a and 10).

The AHW ensemble has a marked negative intensity error through the first 36 h of the forecast (Figs. 9b,c). The negative intensity error begins with an initial vortex that is much too weak, by nearly 100 kt and 80 hPa, in the GEFS reforecast initial analysis. The AHW did intensify TC Rita through the first 48 h of the model integration until landfall, but clearly, the TC intensity is too weak throughout much of the forecast. Within the ensemble, there is some indication that the members with a weaker vortex by 48 h kept TC Rita on a more westward course for a longer period (Figs. 9a,b). The correlation between minimum sea level pressure (MSLP) and TC motion at 48 h is −0.75, indicating that the ensemble members with a stronger TC have an earlier recurvature and landfall farther north along the Texas coastal zone.

In the first subsection below, we will examine the ensemble-mean synoptic-scale flow errors that impacted the environment flow in which TC Rita was embedded. In the second subsection, we will examine the impact of intensity on the track of TC Rita within the ensemble forecast.

a. Environment wind errors

The 24-h AHW forecast $\mathbf{v}_{\text{env}}$ for representative ensemble members (control, left perturbation, and right perturbation) is compared to CFSR in Fig. 11. Note that while there are some differences among the three AHW ensemble members, they are all characterized by well-defined zonal-wind errors with an easterly $\mathbf{v}_{\text{env}}$ error below and westerly $\mathbf{v}_{\text{env}}$ error above 550 hPa compared to the CFSR. Inspection of the 850–500-hPa layer–mean relative vorticity and $\mathbf{v}_{\text{env}}$ shows that the CFSR has weaker low- and midlevel easterlies compared to the AHW ensemble mean (Fig. 12). The subtropical anticyclone over the southeastern CONUS has a stronger circulation with increased anticyclonic vorticity and its center of circulation is located farther west in the AHW

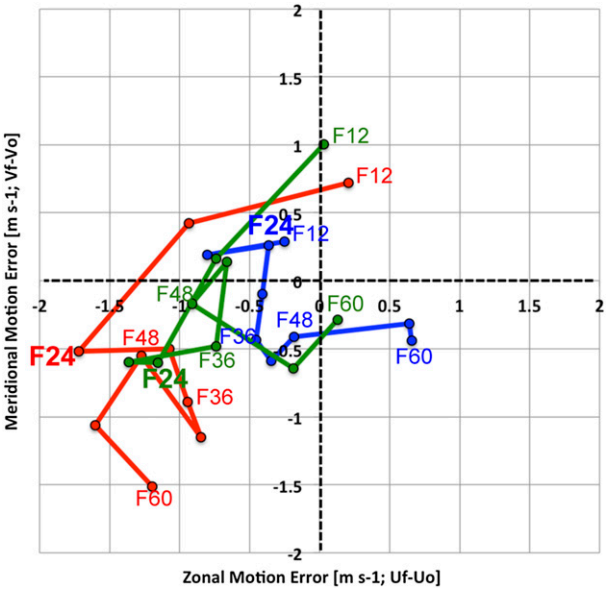

FIG. 10. Scatterplot of the u, v components of TC motion error ($m\,s^{-1}$; AHW forecast minus observed) for the control (green), left (red), and right (blue) perturbation ensemble members at 1200 UTC 22–24 Sep 2005 (12–60-h forecast).

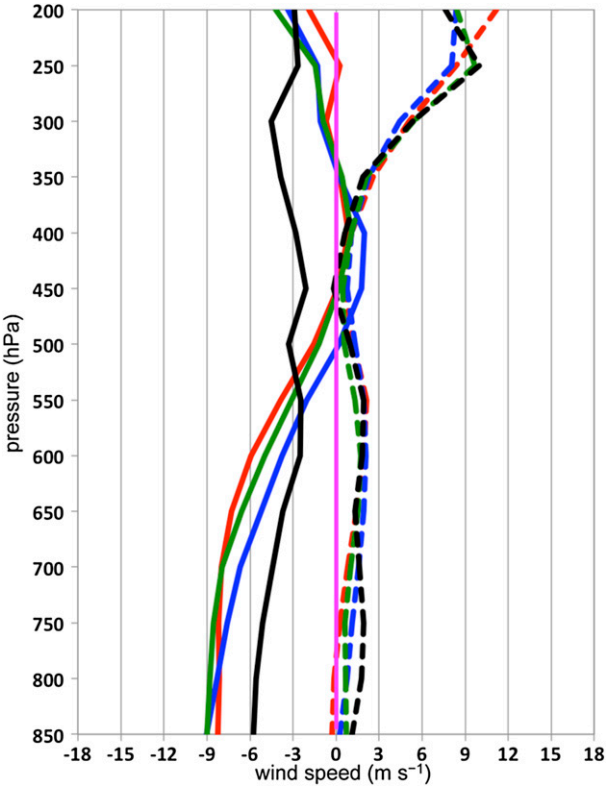

FIG. 11. Vertical profile of $\mathbf{v}_{env}$ speed ($m\,s^{-1}$) components for the CFSR (black) and 24-h AHW control (green), left (red), and right (blue) perturbation ensemble member forecasts verifying at 0000 UTC 23 Sep 2005. The u component is plotted with solid lines and the v component is in dashed lines.

ensemble mean compared to the CFSR (Figs. 12a,b). The AHW ensemble-mean errors in subtropical anticyclone location are highlighted by the 850–500-hPa layer–mean streamfunction error shown in Fig. 13a. Note the anticyclonic flow error over much of the northern Gulf of Mexico and southern Great Plains, indicative of an anticyclone that extends too far south and west in the AHW ensemble-mean forecast. The attendant increased meridional gradient in streamfunction in which TC Rita is embedded is consistent with the easterly $\mathbf{v}_{env}$ error over much of the Gulf of Mexico.

In the 500–200-hPa layer, the 24-h AHW ensemble-mean forecast $\mathbf{v}_{env}$ is characterized by a westerly wind error compared to the CFSR (Fig. 11). Inspection of the relative vorticity and $\mathbf{v}_{env}$ shows that the AHW ensemble has a more circular upper-level anticyclone just west of southern Florida, with reduced anticyclonic vorticity along the Gulf Coast and over northern Florida compared to the CFSR (Figs. 12c,d). The 500–200-hPa streamfunction shows a cyclonic flow error from the northeastern Gulf of Mexico to the Straits of Florida (Fig. 13b). The cyclonic flow error is related to the structure of the upper-level anticyclone east of TC Rita and over the Mississippi River valley and the sharper trough over the extreme southeastern CONUS. In all, the reduced anticyclonic flow aloft northeast of TC Rita contributed to the westerly $\mathbf{v}_{env}$ error aloft. The implication is that in the AHW ensemble forecast there was increased westerly vertical wind shear in TC Rita's environment. In that synoptic-scale flow situation, errors in the vertical structure of a TC will impact the track, where a shallow weak TC will move westward in the easterly flow and a deep strong TC will be impacted by the westerly flow aloft and move more slowly westward and recurve.

b. *Intensity and steering-layer depth errors*

The steering-layer depth and TC motion for the 24- and 48-h AHW ensemble forecasts and verifying CFSR at 0000 UTC 23 and 24 September 2005 are shown in Fig. 14. All but one of the AHW ensemble members have a shallower steering-layer depth compared to the CFSR at 0000 UTC 23 September. Figure 15a shows that the AHW ensemble has the lowest mean absolute difference between steering-layer flow and TC motion for a removal radius of 2° and an 850–450-hPa vertical layer, with a secondary minimum for a removal radius of 4° and an 850–500-hPa layer. By 0000 UTC 24 September, the AHW ensemble members follow a deeper steering-layer flow (Fig. 14). The lowest mean absolute difference between steering-layer flow and TC motion deepens to the 850–300-hPa layer and a 3° removal radius, which is more consistent with the CFSR (Fig. 15b).

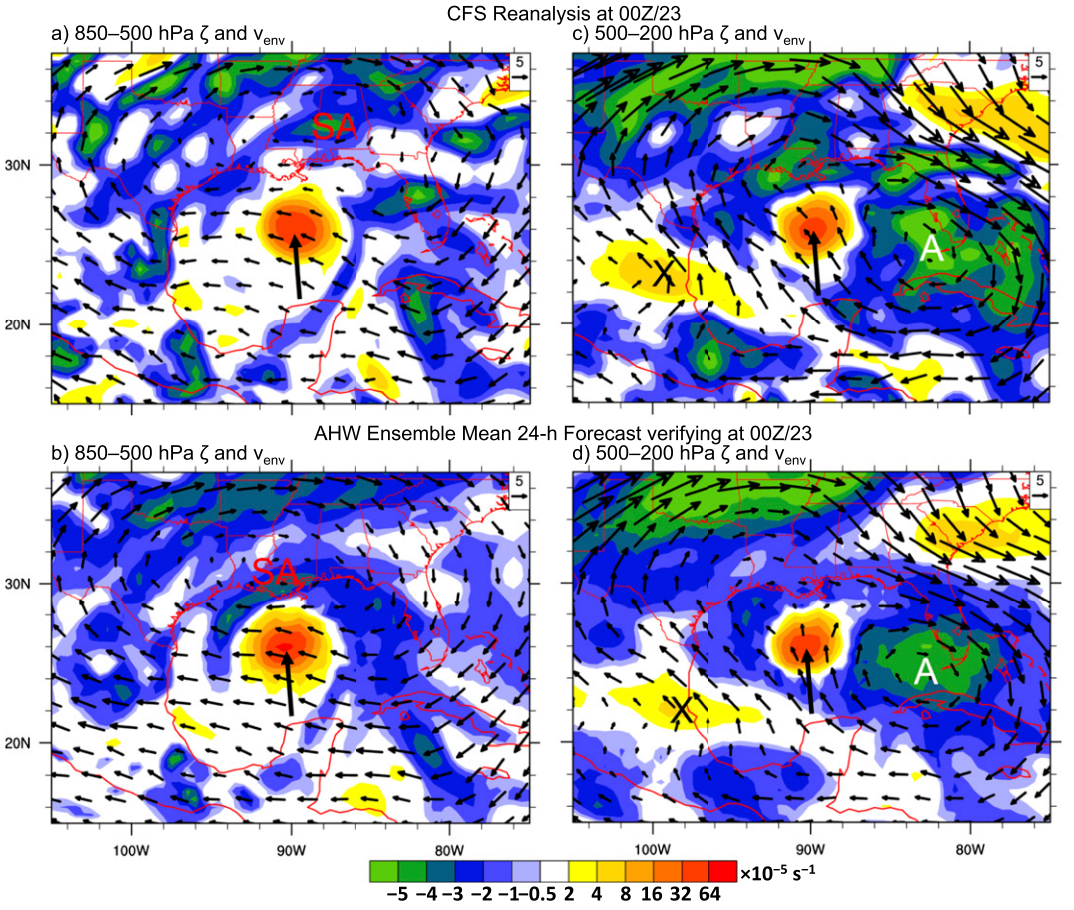

FIG. 12. CFSR (a) 850–500- and (c) 500–200-hPa layer–mean relative vorticity ($\times 10^{-5}\,s^{-1}$; shaded according to the color bar) and $\mathbf{v}_{env}$ ($m\,s^{-1}$; arrows) at 0000 UTC 23 Sep 2005. (b),(d) As in (a),(c), but for the 24-h AHW ensemble-mean forecast. The key synoptic-scale circulation features are labeled as in Fig. 4.

Within the ensemble, the members that follow a deeper steering-layer flow move on a more northwestward course consistent with the observed TC, with the relationship between steering-layer depth and TC motion explaining 50% of the variance in the ensemble (Fig. 14). The correlation between TC minimum sea level pressure and steering-layer depth was −0.65, indicating that stronger TCs follow a deeper steering layer in the ensemble.

The key result here is that all of the AHW ensemble forecasts are initialized with a TC that is too weak and shallow (Figs. 9b,c). By 24 h, these TCs have a southwestward motion error because they are sensitive to a shallower steering-layer flow that is characterized by an easterly wind error (Fig. 11). The ensemble members that are able to intensify the TC more readily produce a better forecast. As an example, the structure and intensity of TC Rita in the AHW 4-km nest for the left and right perturbation ensemble member forecasts is shown in Figs. 16 and 17. In the time–radius plot of 850-hPa vertical velocity and wind speed, the left perturbation forecast is slow to intensify TC Rita compared to the right perturbation forecast (Fig. 16). At 0000 UTC 23 September, the left perturbation forecast has 850-hPa wind speeds near 35 $m\,s^{-1}$ while the right perturbation forecast has wind speeds over 40 $m\,s^{-1}$. Ascent within a radius of 100 km is more organized in the right perturbation forecast by 0000 UTC 23 September. The vertical structure of tangential and radial wind components shows that the right perturbation forecast has a deeper, upright vortex that is consistent with a deeper steering-layer flow (Figs. 17a,c and 15a). By 0000 UTC 24 September, the left perturbation forecast is intensifying, but is still a bit weaker than the right perturbation forecast (Fig. 16). The vertical structure of the two ensemble members are in better agreement, although the right perturbation forecast is more intense through a deep layer, with tangential wind speeds over 70 $m\,s^{-1}$ near 50-km radius (Figs. 17b,d).

In summary, while all of the AHW ensemble members were too weak initially, the members that were able to intensify more quickly and follow a deeper steering-layer

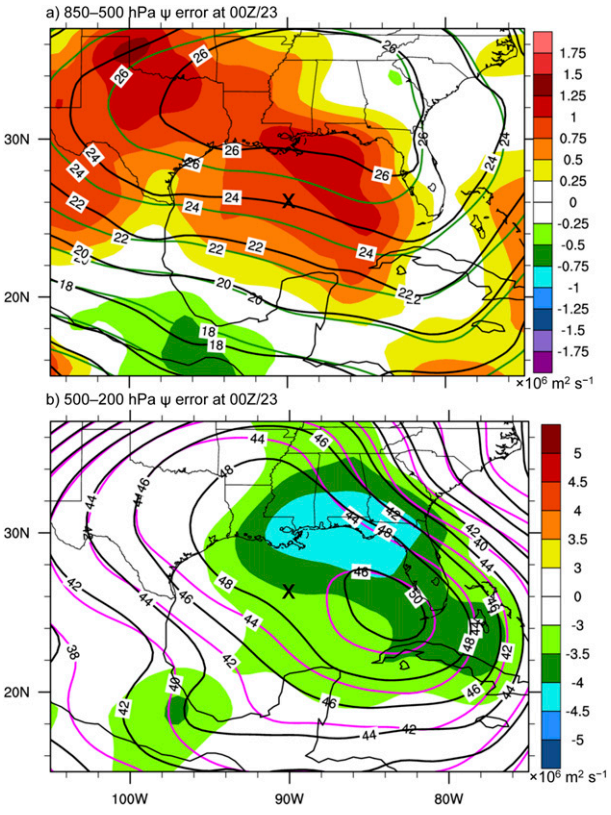

FIG. 13. Streamfunction ($\times 10^6\,m^2\,s^{-1}$; solid contours with an interval of $2.0 \times 10^6\,m^2\,s^{-1}$; CFSR in black; 24-h AHW ensemble-mean forecast colored) and streamfunction error (24-h AHW ensemble-mean forecast minus CFSR; $\times 10^6\,m^2\,s^{-1}$; shaded according to the color bar) at 0000 UTC 23 Sep 2005 for the (a) 850–500- and (b) 500–200-hPa layers. The streamfunction was computed using $\mathbf{v}_{env}$.

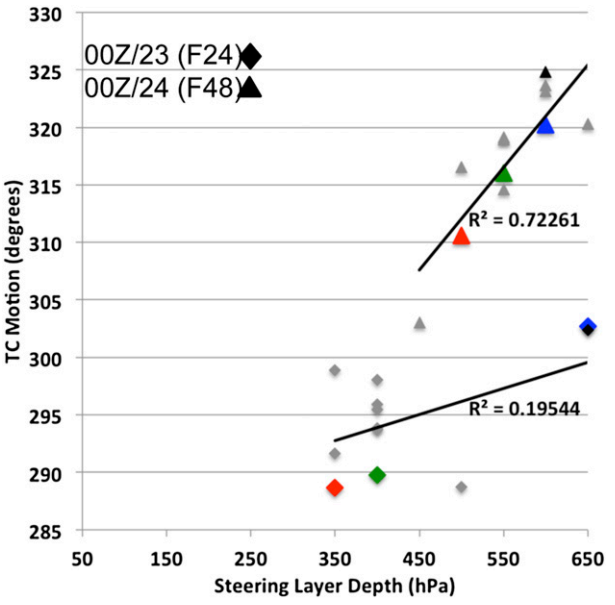

FIG. 14. Scatterplot of steering-layer depth (hPa; *x* axis) and TC motion (°; *y* axis) for the 24- (diamonds) and 48-h (triangles) AHW ensemble forecasts verifying at 0000 UTC 23 and 24 Sep 2005, respectively. The observed TC is black filled and AHW ensemble members are gray filled. The control, left, and right perturbation ensemble members are filled in green, red, and blue, respectively. The trend lines and coefficient of determination R^2 values are indicated.

flow moved on a more northwestward course in better agreement with the observed TC. To test this assertion further, the predicted TC tracks for different steering-layer flow definitions using the wind field from the CFSR and from the AHW control member at 1200 UTC 22–24 September 2005 are shown in Fig. 18. This calculation assumes that an individual TC starts at the observed position at 1200 UTC 22 September and follows the same steering-layer definition (depth and radius) for the entire period. For both the CFSR and AHW control member, the better track forecasts are those TCs that follow a steering layer ≥500 hPa deep. This result highlights the importance of accurately initializing the TC vortex in numerical weather prediction forecasts, particularly in situations where the numerical model has a westerly wind shear error in the environment flow.

6. Concluding discussion

The aim of this study was to examine and diagnose the short- to medium-range track forecast errors for TC Rita (2005) in the 2–4-day period prior to its landfall along the Texas–Louisiana coastal zone. The operational numerical weather prediction guidance initialized at 0000 UTC 20–22 September 2005, 2–4 days prior to landfall, all exhibited a left-of-track error with the primary threat for landfall located near the Houston, Texas, area. The largest mass evacuation in U.S. history was ordered, which produced more fatalities than the storm itself. Given the persistent left-of-track forecast errors and overall socioeconomic impacts, analysis and diagnosis of the track forecast errors for TC Rita are worthy of study within the context of the climatological forecast track errors in the Gulf of Mexico region.

In this study, we utilize the GEFS reforecast dataset that was generated using the February 2012 version of the operational GEFS (Hamill et al. 2013). Through February 2011, the GEFS reforecasts used the CFSR (Saha et al. 2010) as initial conditions, and employed the operational analyses thereafter. While reforecasts in general are quite useful for collectively examining a long time series of forecasts of relatively rare events, they are also beneficial within the case study framework. Herein, we analyze and diagnose track forecasts for TC Rita from the GEFS reforecasts to determine the key factors that contributed to the left-of-track forecast error prior to TC Rita's landfall.

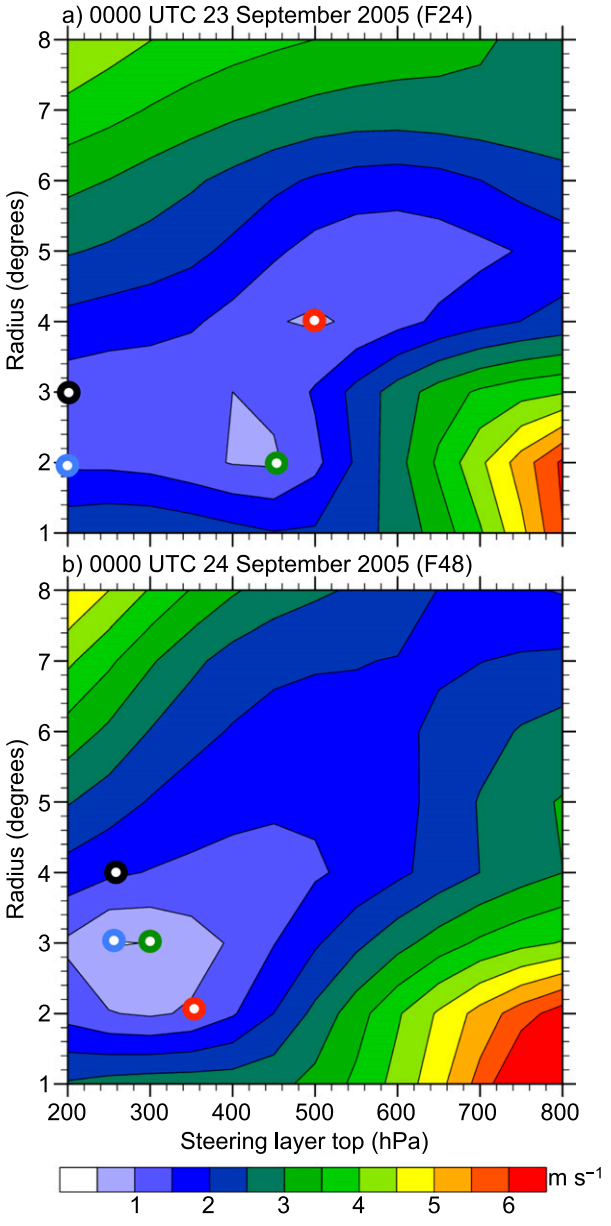

FIG. 15. AHW forecast ensemble-mean absolute vector wind difference ($m\,s^{-1}$; shaded according to the color bar) between the TC motion and steering-layer flow as a function of vertical depth (hPa; x axis) and TC removal radius (°; y axis) verifying at 0000 UTC (a) 23 and (b) 24 Sep 2005. The steering-layer flow definitions for the observed and the control, left, and right perturbation AHW ensemble members are shown by the white-filled black, green, red, and blue circles, respectively.

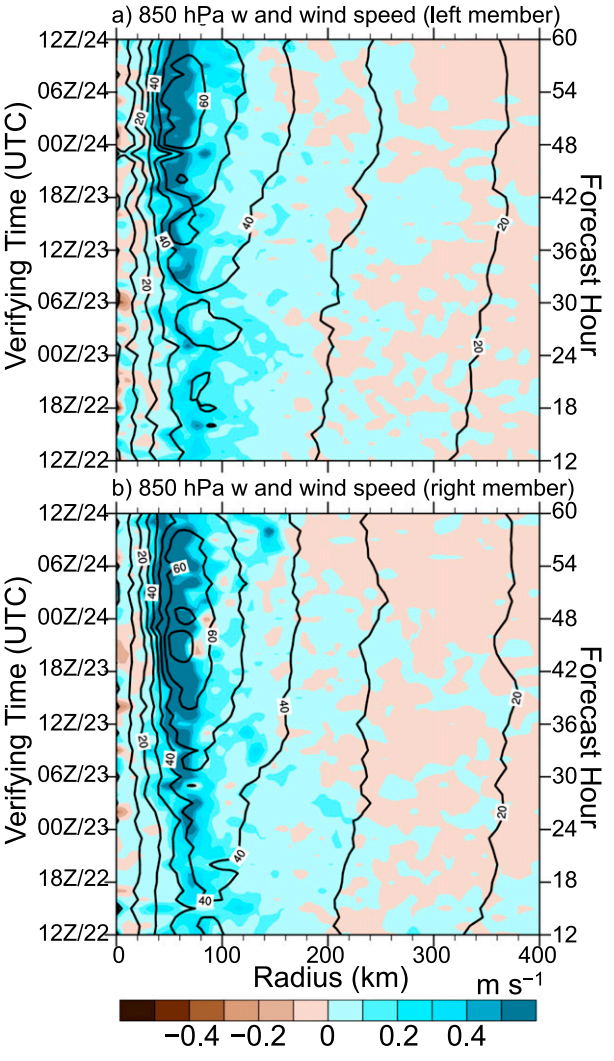

FIG. 16. Time–radius plot of azimuthal mean 850-hPa wind speed ($m\,s^{-1}$; black contours with an interval of $10\,m\,s^{-1}$) and vertical velocity ($m\,s^{-1}$; shaded according to the color bar) for the 12–60-h (a) left and (b) right perturbation AHW ensemble member forecasts verifying at 1200 UTC 22–24 Sep 2005. These were generated from the explicit 4-km inner nest.

Much like the operational forecasts, the GEFS reforecasts were characterized by a persistent left-of-track error in the 2–4-day period prior to TC Rita's landfall. Employing a time-lagged ensemble approach similar to that used by Schumacher and Galarneau (2012), it was determined that the left-of-track error in the ensemble was driven by errors in the synoptic-scale flow. Specifically, the subset of ensemble members from the 0000 UTC 20–22 September 2005 initializations that maintained a more westward course ("nonrecurving" members) toward Texas rather than recurved ("recurving" members) toward the Texas–Louisiana border were characterized by a subtropical anticyclone that extended too far south and west over the southern CONUS and northwestern Gulf of Mexico. The sensitivity of TC Rita's track to the westward extent of the subtropical anticyclone bears similarity to the track forecasts for TC Ike (2008) analyzed by Brennan and Majumdar (2011).

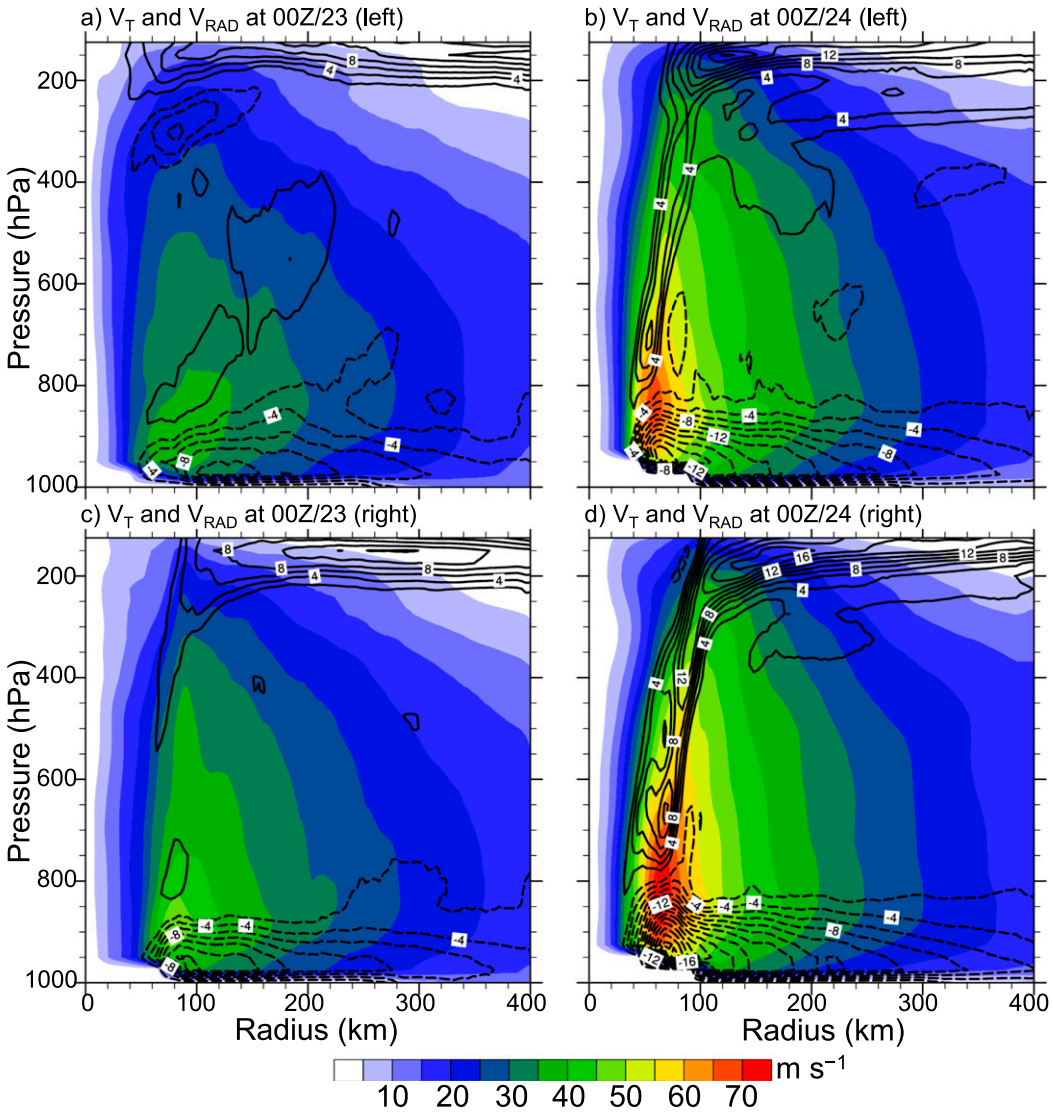

FIG. 17. Pressure–radius plot of azimuthal mean tangential (m s^{-1}; shaded according to the color bar) and radial wind (m s^{-1}; black contours with an interval of 2 m s^{-1}, where solid contours indicate outflow, dashed contours indicate inflow, and the zero contour is omitted) for the 24-h (a) left and (c) right perturbation AHW ensemble member forecasts verifying at 0000 UTC 23 Sep 2005. (b),(d) As in (a),(c), but for the 48-h forecast verifying at 0000 UTC 24 Sep 2005. These were generated from the explicit 4-km inner nest.

Inspection of the GEFS reforecasts also showed that TC Rita's forecast track was sensitive to an upper-level cutoff low west and anticyclone east of TC Rita. The cutoff low was instrumental in TC Rita's initial development over the western North Atlantic, moved westward, and was located over eastern Mexico by 22 September. The upper-level anticyclone east of TC Rita amplified over the eastern Gulf of Mexico ahead of a weak trough over the southeastern CONUS, and was likely further amplified by diabatically enhanced anticyclogenesis that accompanied TC Rita's rapid intensification. The nonrecurving ensemble members had a weaker cutoff low and anticyclone, with an attendant reduced southerly flow at upper levels and increased easterly flow at midlevels over TC Rita. The recurving ensemble members had more robust southerly flow at upper levels and reduced easterly flow at midlevels, which steered TC Rita on a more northwestward course.

In addition to the GEFS reforecasts, analysis of an AHW regional reforecast ensemble initialized at 0000 UTC 22 September 2005 was performed to assess how increased model resolution and forecasted vortex structure impacted the track forecast. The track

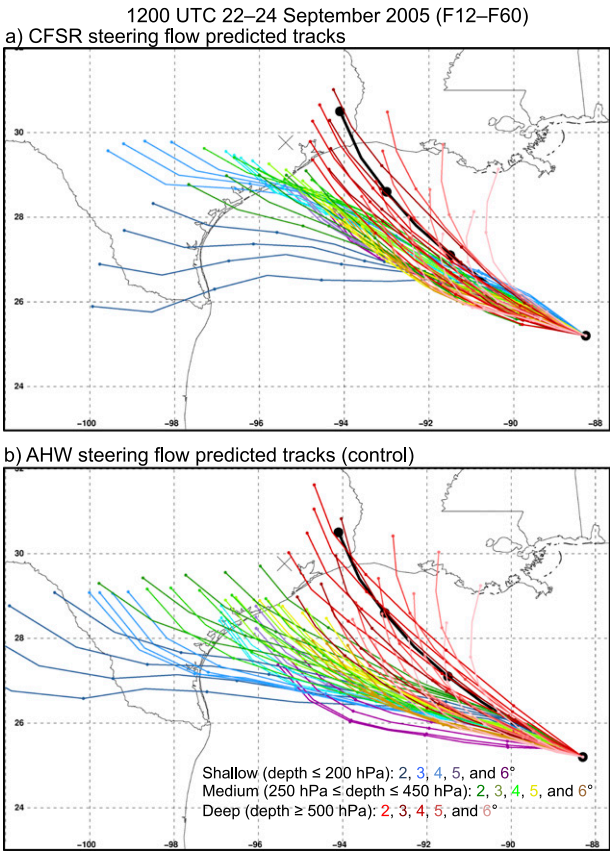

FIG. 18. Predicted tracks of TC Rita at 1200 UTC 22–24 Sep 2005 starting at the observed TC position and using different steering-layer flow definitions as a function of TC removal radius and vertical depth based on the (a) CFSR and (b) AHW control member environment wind field. The predicted tracks are colored according to the key in (b). The TC positions are marked every 12 h by a filled circle.

forecasts showed a similar left-of-track error as the GEFS reforecasts, indicating that increased model resolution (and a different modeling system) did not significantly change the track forecast. Inspection of the AHW ensemble-mean synoptic-scale flow showed that the forecasts were characterized by a subtropical ridge that extended too far south and west, much like in the GEFS reforecasts, which drove an easterly environment wind error at low to midlevels. Additionally, reduced ridging in the forecast northeast of TC Rita was associated with a westerly wind error in the mid- to upper levels. The westerly vertical wind shear error in the AHW ensemble increased the sensitivity of TC Rita's track to the steering-layer (and vortex) depth.

In addition to errors in the synoptic-scale flow, the forecasted track of TC Rita in the AHW ensemble was also sensitive to the intensity and steering-layer depth. All of the ensemble members were initialized with a TC vortex that was too shallow and weak. The initial vortex from the CFSR had an MSLP of 980 hPa, whereas the observed TC was near 900 hPa at 0000 UTC 22 September. The explicit 4-km inner nest was able to intensify the TC vortex to an intensity comparable to observations by 48 h. The AHW ensemble members that were able to intensify TC Rita more rapidly early in the forecast produced a better track forecast as the more intense TCs responded to a deeper steering-layer flow. In fact, the predicted tracks based on steering-layer flow as a function of TC removal radius and vertical depth showed that deeper steering-layer flows produced better track forecasts regardless of whether the AHW ensemble-mean forecast or CFSR wind fields were used (Fig. 18). It is likely that the optimal steering layer is sensitive to the structure of both the TC vortex and the convectively generated outflow, where the former responds to the environment flow and the latter modifies the environment flow (e.g., Tripoli 2014). Untangling the relative importance of these structures in TC motion requires the idealized framework, such as recent work by Fovell and Su (2007) and Fovell et al. (2009) that tested the impact of different microphysical parameterizations on TC radial structure and motion.

The track forecasts for TC Rita by the GEFS reforecast and AHW regional reforecast ensembles were both consistent with the GEFS reforecast climatology of track forecast errors over the Gulf of Mexico for 1985–2010. These forecasts, whose mean absolute track errors were consistent with the HFIP baseline, were characterized by a medium-range left-of-track forecast bias. In addition, while not surprising given the relatively coarse resolution of the global model, the intensity forecasts had a negative bias. As demonstrated in the analysis of forecasts for TC Rita, the negative intensity bias, in concert with errors in the synoptic-scale flow, may play a key role in the climatological left-of-track error in the region.

The value of improved initial conditions in TC track forecasts is well documented. Hamill et al. (2011a,b) showed that improved initial conditions that accompanied the ensemble Kalman filter (EnKF) and hybrid[4] data assimilation systems led to improved GEFS TC track forecasts compared to the operational GEFS that used the Global Statistical Interpolation analysis system (GSI). The hybrid system has since been incorporated into operations at NCEP. The CFSR, used to initialize the GEFS reforecasts through February 2011, employed the older GSI. The operational GEFS for 2012–14,

[4] The hybrid data assimilation system uses a blend of GSI background covariances and EnKF covariances. A full description is provided by Hamill et al. (2011b, p. 3244).

which is the same model version as the GEFS reforecasts except using the new hybrid data assimilation system, still shows a left-of-track bias for 12–60-h forecast leads in the Gulf of Mexico region (not shown). The magnitude of the left-of-track bias is reduced compared to the GEFS reforecasts for 1985–2010, suggesting that advancements in data assimilation may have contributed to improved TC track predictions in the region. However, that the operational GEFS for 2012–14 has a similar TC track forecast bias in the Gulf of Mexico region as the GEFS reforecasts suggests that the TC Rita case study presented herein highlights aspects of the TC forecast problem that can continue to be addressed with newer modeling systems.

A possible future study would be to generate a new set of global analyses for the 2005 TC season using the hybrid or EnKF data assimilation systems. While overall improvements in the synoptic-scale flow will likely be small over data-rich North America, any improvements in initial TC structure that reduce the climatological negative intensity bias apparent in the GEFS reforecast initial conditions may help lessen or eliminate the persistent left-of-track error for TC Rita and other cases.

Acknowledgments. Research support was provided by NOAA HFIP Award NA12NWS4680005. We thank George Bryan (NCAR) for his valuable comments on the manuscript. We also thank Gary Bates (NOAA/ESRL) for providing technical support and Mike Fiorino (NOAA/ESRL) for generating the GEFS TC forecast tracks. Three anonymous reviewers are thanked for their helpful comments on the manuscript.

REFERENCES

Brennan, M. J., and S. J. Majumdar, 2011: An examination of model track forecast errors for Hurricane Ike (2008) in the Gulf of Mexico. *Wea. Forecasting*, **26**, 848–867, doi:10.1175/WAF-D-10-05053.1.

Buckingham, C., T. Marchok, I. Ginis, L. Rothstein, and D. Rowe, 2010: Short- and medium-range prediction of tropical and transitioning cyclone tracks within the NCEP Global Ensemble Forecasting System. *Wea. Forecasting*, **25**, 1736–1754, doi:10.1175/2010WAF2222398.1.

Carr, L. E., and R. L. Elsberry, 2000: Dynamical tropical cyclone track forecast errors. Part I: Tropical region error sources. *Wea. Forecasting*, **15**, 641–661, doi:10.1175/1520-0434(2000)015<0641:DTCTFE>2.0.CO;2.

Davis, C. A., W. Wang, J. Dudhia, and R. Torn, 2010: Does increased horizontal resolution improve hurricane wind forecasts? *Wea. Forecasting*, **25**, 1826–1841, doi:10.1175/2010WAF2222423.1.

Ek, M. B., K. E. Mitchell, Y. Lin, E. Rogers, P. Grunmann, V. Koren, G. Gayno, and J. D. Tarpley, 2003: Implementation of Noah land surface model advances in the National Centers for Environmental Prediction operational mesoscale Eta Model. *J. Geophys. Res.*, **108**, 8851, doi:10.1029/2002JD003296.

Fovell, R. G., and H. Su, 2007: Impact of cloud microphysics on hurricane track forecasts. *Geophys. Res. Lett.*, **34**, L24810, doi:10.1029/2007GL031723.

——, K. L. Corbosiero, and H.-C. Kuo, 2009: Cloud microphysics impact on hurricane track as revealed in idealized experiments. *J. Atmos. Sci.*, **66**, 1764–1778, doi:10.1175/2008JAS2874.1.

Galarneau, T. J., Jr., and C. A. Davis, 2013: Diagnosing forecast errors in tropical cyclone motion. *Mon. Wea. Rev.*, **141**, 405–430, doi:10.1175/MWR-D-12-00071.1.

Gall, R., F. Toepfer, F. Marks, and E. Rappaport, 2014: National Oceanic and Atmospheric Administration Hurricane Forecast Improvement Project years five to ten strategic plan. Tech. Rep. HFIP2014-1.1a, NOAA/Hurricane Forecast Improvement Project, 44 pp. [Available online at http://www.hfip.org/documents/HFIP_StrategicPlan_Yrs5-10_Nov05_2014_Update.pdf.]

Hakim, G. J., and R. D. Torn, 2008: Ensemble synoptic analysis. *Synoptic–Dynamic Meteorology and Weather Analysis and Forecasting: A Tribute to Fred Sanders*, *Meteor. Monogr.*, No. 55, Amer. Meteor. Soc., 147–161.

Hamill, T. M., J. S. Whitaker, M. Fiorino, and S. G. Benjamin, 2011a: Global ensemble predictions of 2009's tropical cyclones initialized with an ensemble Kalman filter. *Mon. Wea. Rev.*, **139**, 668–688, doi:10.1175/2010MWR3456.1.

——, ——, D. T. Kleist, M. Fiorino, and S. G. Benjamin, 2011b: Predictions of 2010's tropical cyclones using the GFS and ensemble-based data assimilation methods. *Mon. Wea. Rev.*, **139**, 3243–3247, doi:10.1175/MWR-D-11-00079.1.

——, G. T. Bates, J. S. Whitaker, D. R. Murray, M. Fiorino, T. J. Galarneau Jr., Y. Zhu, and W. Lapenta, 2013: NOAA's second-generation global medium-range ensemble reforecast dataset. *Bull. Amer. Meteor. Soc.*, **94**, 1553–1565, doi:10.1175/BAMS-D-12-00014.1.

Hong, S.-Y., J. Dudhia, and S.-H. Chen, 2004: A revised approach to ice microphysical processes for the bulk parameterization of clouds and precipitation. *Mon. Wea. Rev.*, **132**, 103–120, doi:10.1175/1520-0493(2004)132<0103:ARATIM>2.0.CO;2.

——, Y. Noh, and J. Dudhia, 2006: A new vertical diffusion package with an explicit treatment of entrainment processes. *Mon. Wea. Rev.*, **134**, 2318–2341, doi:10.1175/MWR3199.1.

Horswell, C., and E. Hegstrom, 2005: Exodus weighs heavily in death toll: 107. *Houston Chronicle*, accessed 2 March 2015. [Available online at http://www.chron.com/news/hurricanes/article/Exodus-weighs-heavily-in-death-toll-107-1502590.php.]

Knabb, R. D., D. P. Brown, and J. R. Rhome, 2006: Tropical cyclone report: Hurricane Rita. Tech. Rep. AL182005, NOAA/National Hurricane Center, 33 pp. [Available online at http://www.nhc.noaa.gov/data/tcr/AL182005_Rita.pdf.]

Komaromi, W. A., S. J. Majumdar, and E. D. Rappin, 2011: Diagnosing initial condition sensitivity of Typhoon Sinlaku (2008) and Hurricane Ike (2008). *Mon. Wea. Rev.*, **139**, 3224–3242, doi:10.1175/MWR-D-10-05018.1.

Landsea, C., and Coauthors, 2004: The Atlantic Hurricane Database reanalysis project: Documentation for the 1851–1910 alterations and additions to the HURDAT database. *Hurricanes and Typhoons: Past, Present, and Future*, R. J. Murname and K.-B. Liu, Eds., Columbia University Press, 177–221.

Majumdar, S. J., S. D. Aberson, C. H. Bishop, R. Buizza, M. S. Peng, and C. A. Reynolds, 2006: A comparison of adaptive observing guidance for Atlantic tropical cyclones. *Mon. Wea. Rev.*, **134**, 2354–2372, doi:10.1175/MWR3193.1.

Mitchell, C. L., 1924: West Indian hurricanes and other tropical cyclones of the North Atlantic Ocean. U.S. Weather Bureau Suppl. 24, 47 pp.

Saha, S., and Coauthors, 2010: The NCEP Climate Forecast System Reanalysis. *Bull. Amer. Meteor. Soc.*, **91**, 1015–1057, doi:10.1175/2010BAMS3001.1.

Schumacher, R. S., and T. J. Galarneau Jr., 2012: Moisture transport into midlatitudes ahead of recurving tropical cyclones and its relevance in two predecessor rain events. *Mon. Wea. Rev.*, **140**, 1810–1827, doi:10.1175/MWR-D-11-00307.1.

Simpson, R. H., 1974: The hurricane disaster–potential scale. *Weatherwise*, **27**, 169–186, doi:10.1080/00431672.1974.9931702.

Skamarock, W. C., and Coauthors, 2008: A description of the Advanced Research WRF version 3. NCAR Tech. Note NCAR/TN–475+STR, 125 pp. [Available online at http://www2.mmm.ucar.edu/wrf/users/docs/arw_v3.pdf.]

Torn, R. D., and C. A. Davis, 2012: The influence of shallow convection on tropical cyclone track forecasts. *Mon. Wea. Rev.*, **140**, 2188–2197, doi:10.1175/MWR-D-11-00246.1.

——, J. S. Whitaker, P. Pegion, T. M. Hamill, and G. J. Hakim, 2015: Diagnosis of the source of GFS medium-range track errors in Hurricane Sandy (2012). *Mon. Wea. Rev.*, **143**, 132–152, doi:10.1175/MWR-D-14-00086.1.

Tripoli, G. J., 2014: Tropical cyclone–environment interaction in the ULTS. *Proc. 31st Conf. on Hurricanes and Tropical Meteorology*, San Diego, CA, Amer. Meteor. Soc., 78. [Available online at https://ams.confex.com/ams/31Hurr/webprogram/Paper245207.html.]

Wilks, D. M., 1995: *Statistical Methods in the Atmospheric Sciences: An Introduction.* Academic Press, 467 pp.

Wu, C. C., and Coauthors, 2009: Intercomparison of targeted observation guidance for tropical cyclones in the northwestern Pacific. *Mon. Wea. Rev.*, **137**, 2471–2492, doi:10.1175/2009MWR2762.1.

Zhang, F., and Coauthors, 2007: An in-person survey investigating public perceptions of and responses to Hurricane Rita forecasts along the Texas coast. *Wea. Forecasting*, **22**, 1177–1190, doi:10.1175/2007WAF2006118.1.